# Multiple-peak resonance of optical second harmonic generation arising from band nesting in monolayer transition metal dichalcogenides $TX_2$ on $SiO_2$/Si(001) substrates ($T$ = Mo, W; $X$ = S, Se)

Yuhei Kikuchi,[1] Yoshihiro Miyauchi,[2] Ryosei Takaoka,[1] Takanori Suzuki,[2] Masatoshi Tanaka,[1] and Shinya Ohno[1]
[1]*Department of Physics, Faculty of Engineering, Yokohama National University, 79-5 Tokiwadai, Hodogaya-ku, Yokohama, 240–8501, Japan*
[2]*Department of Applied Physics, National Defense Academy of Japan, 1-10-20 Hashirimizu, Yokosuka, Kanagawa 239–8686, Japan*

(Received 16 December 2018; revised manuscript received 8 July 2019; published 6 August 2019; corrected 5 September 2019)

The nonlinear optical response of monolayer transition-metal dichalcogenides $TX_2$ ($T$ = Mo, W; $X$ = S, Se) on $SiO_2$/Si(001) substrates was examined using second-harmonic generation (SHG) spectroscopy in combination with differential reflectance (DR) spectroscopy. In the SHG spectroscopy, the second-harmonic intensity corrected by a crystalline quartz reference was obtained for the wavelength of the incident femtosecond laser varied from 750 to 1040 nm. The SHG spectra of all the four $TX_2$ were dominated by two-photon resonance around the C peaks in the DR spectra that was previously assigned to interband transitions at critical points formed as a result of band nesting. Multiple peaks were observed in each resonance spectrum, which was then decomposed into a few components. The overall feature of the main components—denoted as $\overline{C1}$ and $\overline{C2}$—was common among the four $TX_2$ materials. The optical transitions contributing to these components were concluded to occur at different $k$ points in a ring-shaped area around the Γ point with the aid of the published results of optical spectrum calculations and the SHG spectrum of bilayer $MoS_2$. In addition, one-photon resonance at the $A$ exciton and two-photon resonance at the $A'$ exciton were observed in $MoSe_2$ and $WSe_2$, respectively, and their intensities were proven to be significantly lower than those of the resonances around the C peaks.

DOI: 10.1103/PhysRevB.100.075301

## I. INTRODUCTION

Atomically thin layered materials have attracted considerable attention since graphene was found to have novel physical properties [1]. Among them, group 6 transition-metal dichalcogenides $TX_2$ ($T$ = Mo, W; $X$ = S, Se) are considered as promising semiconductors having controllable bandgaps in the visible region [2–4] and have drawn significant research interest for electronic and optoelectronic device applications [5–8]. Monolayer $TX_2$ is also interesting from a scientific perspective as a two-dimensional model system for exploring the characteristics of nanostructures, such as anomalous lattice vibration [9,10], the transition from indirect- to direct-bandgap semiconductors [11,12], and spin-valley dynamics [13,14].

Most linear optical studies on monolayer $TX_2$ [15–19] have focused on the exciton peaks at absorption edges, which are conventionally denoted as A and B [20]. The dielectric functions in the exciton region suggest apparent absorption with a peak absorbance of 0.05 even in a monolayer [16]. On the other hand, the absorbance of the peak around 3 eV due to interband transitions, which is conventionally denoted as C [20], is approximately three times larger than that of the exciton peaks, and the bandwidth of peak C is approximately 10 times larger than that of the exciton peaks. Therefore, the interband transition region plays an important role in photonics and optoelectronics applications. The strong light-matter interaction in this region was ascribed to band nesting [21]. Band nesting means that the conduction and valence bands are parallel to each other in the band structure plot, which results in van Hove singularities in the joint density of states (JDOS) function. In low-dimensional systems, the JDOS diverges at the singularities, yielding high optical conductivities. The importance of the band nesting in the light-matter interaction was experimentally demonstrated in a dynamical study on photocarrier relaxation pathways [22]. It was also predicted that the nonlinear optical response in the interband transition region is strong because the trigonal prismatic structure of monolayer $TX_2$ lacks inversion symmetry [21].

The nonlinear optical properties of mono- and few-layer $TX_2$, especially the second-harmonic generation (SHG), have been studied using optical microscopy for $MoS_2$ [23–27], for $MoSe_2$ [26], for $WS_2$ [26,28,29], and for $WSe_2$ [26–30]. It was pointed out [29] that the estimated second-order nonlinear optical susceptibility ($\chi^{(2)}$) is as high as 1 nm/V and approximately three orders of magnitude higher than that of common nonlinear optical crystals such as BBO. The photon-energy dependence of the second-harmonic (SH) intensity (SHG spectra) was first measured in the interband transition region for $MoS_2$ [31] and was later measured in the exciton region for $MoS_2$ [32,33], for $MoSe_2$ [34,35], for $WS_2$ [36,37], and for $WSe_2$ [38,39]. Theoretical calculations provided SHG spectra in a wider region of several tenths of eV to several eV [29,32,40–43]. However, knowledge regarding the SHG spectra in the interband transition region, where a larger SHG is expected, is still limited. The authors of Ref. [31] reported the SHG spectra of mono- and three-layer $MoS_2$. This is the only experimental study on the SHG spectra in the interband transition region, to the best of our knowledge. Their SHG spectra appeared to shift to higher energies compared with the

 ©2019 American Physical Society

differential reflectance (DR) spectra; however, the difference was not mentioned in the article. If we measure the SHG spectra of other $TX_2$ materials and compare them with the corresponding DR spectra, the cause of the difference can be elucidated, because the relationship between the photoluminescence excitation spectra and DR spectra is diverse among the four $TX_2$ materials [22]. Moreover, the $\chi^{(2)}$ of monolayer $TX_2$ in the exciton region and the interband transition region have been evaluated separately and with some uncertainty; thus, the ratio of $\chi^{(2)}$ in the two regions is still unclear. A direct comparison of the SH intensity in the interband transition region with that in the exciton region will provide information useful for the application of $TX_2$ materials to nonlinear optical devices.

In a previous study [44], we measured the SHG spectra of few-layer $MoSe_2$ using a homemade SHG microscope and evaluated the performance of the measurement system. In the present study, we measured the precise SHG spectra of monolayer group 6 transition-metal dichalcogenides ($TX_2$, $T = \mathrm{Mo},\ \mathrm{W};\ X = \mathrm{S},\ \mathrm{Se}$) on $SiO_2$/Si(001) substrates in the two-photon energy region of 2.4–3.3 eV at the average interval of 0.017 eV. The SHG spectra were compared with the DR spectra measured using a homemade DR microscope. The precise SHG spectra allowed us to elucidate the origin of the features of the SHG spectra and thus clarify the cause of the difference between the SHG spectra and the DR spectra previously observed for $MoS_2$, as well as to directly compare the SH intensities in the interband transition region with those in the exciton region for $MoSe_2$ and $WSe_2$. The information obtained is indispensable for the application of monolayer $TX_2$ to nonlinear optical devices.

## II. EXPERIMENTAL PROCEDURE

Monolayer $TX_2$ flakes were mechanically exfoliated from single crystals on a 90-nm-thick $SiO_2$-coated Si(001) substrate. The crystals used in the measurements were naturally grown $MoS_2$, $MoSe_2$ grown via $Br_2$ vapor transport, and $WS_2$ and $WSe_2$ grown via vapor transport without a transport agent [45]. The number of layers was identified using an atomic force microscope (Bruker Innova). For the SHG measurements, the fundamental pulse from a Ti:sapphire oscillator (Spectra Physics Maitai-HP, pulse duration of 80 fs, wavelength of 750–1040 nm, repetition rate of 80 MHz, power of 3 W) passed through a polarizer and a low-pass filter, was reflected by a dichroic dielectric-multilayer mirror inside of an optical microscope (Nikon, Y-FL), and was focused by an objective lens (Nikon LU plan × 100, NA 0.9) onto a sample. The pulse durations of fundamental light were monitored by using a spectrum analyzer (Ocean Photonics, LSM-mini). The light at the double frequency emitted from the sample passed through the objective lens, the dichroic mirror, a high-pass filter, a polarizer, and a monochromator and was detected by a photomultiplier tube [44]. The SH light was expected to have a spectral bandwidth of approximately 4 nm (approximately 0.03 eV at 3 eV) because the bandwidth of the fundamental pulse was approximately 11 nm. For the dichroic mirrors, we used DM 750 and XF 2033 below and above 1000 nm, respectively, on the basis of their transmittance spectra [46]. SHG spectra were measured using *s*-polarized incident light for 750–1040 nm and *p*-polarized SH light for 375–520 nm, where the *s* and *p* polarizations were defined with respect to the dichroic mirror tilted 45° against the incident light. The SHG spectra were corrected by a crystalline quartz reference placed at the sample position.

When the incident light polarization was parallel to the zigzag direction, the element of the second-order susceptibility tensor $\chi^{(2)}_{xyy} = \chi^{(2)}_{yxy} = \chi^{(2)}_{yyx} = -\chi^{(2)}_{xxx}$, where the $x$ and $y$ axes are along the armchair and zigzag directions, respectively, was observed. The azimuth-angle dependence of the SH intensity measured by keeping the axes of the polarizer and the analyzer parallel to each other exhibited threefold symmetry. SHG spectra were measured with incident light polarized parallel to the zigzag direction and without an analyzer. The interference among the multiply reflected fundamental and SH light beams in the $TX_2/SiO_2/Si$ system did not severely affect peak positions and intensities of the component spectra peaked in the region from 2.6 to 3.1 eV when the thickness of the $SiO_2$ layer is 90 nm. This is demonstrated by the enhancement factor spectrum [44] calculated based on the method [47] developed to explain unusual Raman spectrum of graphene (see Supplemental Material, Ref. [48]).

The DR spectra were measured using broadband emission from a halogen lamp, which was spatially filtered by a rectangular aperture before being focused onto the sample using an objective. The spot diameter on the sample was approximately 2 $\mu$m. Reflected light was collected by the same objective and introduced to a multichannel spectrometer (an Acton SpectraPro 2150i monochromator and a Princeton Instruments PIXIS 256E cooled charge-coupled device) with an optical fiber cable. The reflectance spectrum of the substrate, $R_S$, and that of a $TX_2$ flake on the substrate, $R_{TX2}$, were measured to obtain a DR spectrum $\Delta R/R = (R_S - R_{TX2})/R_S$. The wavelength purity of the DR measurements was 2.2 nm (0.016 eV at 3 eV). All measurements were performed at room temperature in ambient conditions.

## III. RESULTS AND DISCUSSION

The corrected SHG spectra of monolayer $TX_2$ on 90-nm-thick $SiO_2$ coated Si (001) substrates are indicated by blue dots with respect to the two-photon energy in Figs. 1(a)–1(d). Each spectrum is dominated by a resonance curve, resembling the SHG spectrum of monolayer $MoS_2$ in Ref. [31]. The peak energy of our spectrum of $MoS_2$, i.e., 2.93 eV, is almost the same as that of theirs: 2.89 eV. However, our spectrum obviously has a shoulder at 2.82 eV, which was not observed in Ref. [31]. This is probably because our spectra were measured every 0.017 eV on average, whereas the spectra were measured every 0.067 eV in Ref. [31]. Several spectral features are also found on the resonance curves for other $TX_2$ materials.

The SHG spectra were fitted by a linear combination of Lorentz functions in order to decompose the spectra into a few components and determine their peak energies. The linear combination of the Lorentz functions is defined as

$$I(\omega) \propto \sum_{k,l} \left( \frac{f_k^2}{(\omega-\omega_k)^2+(\Gamma_k/2)^2} + \frac{f_l^2}{(2\omega-\omega_l)^2+(\Gamma_l/2)^2} \right), \tag{1}$$

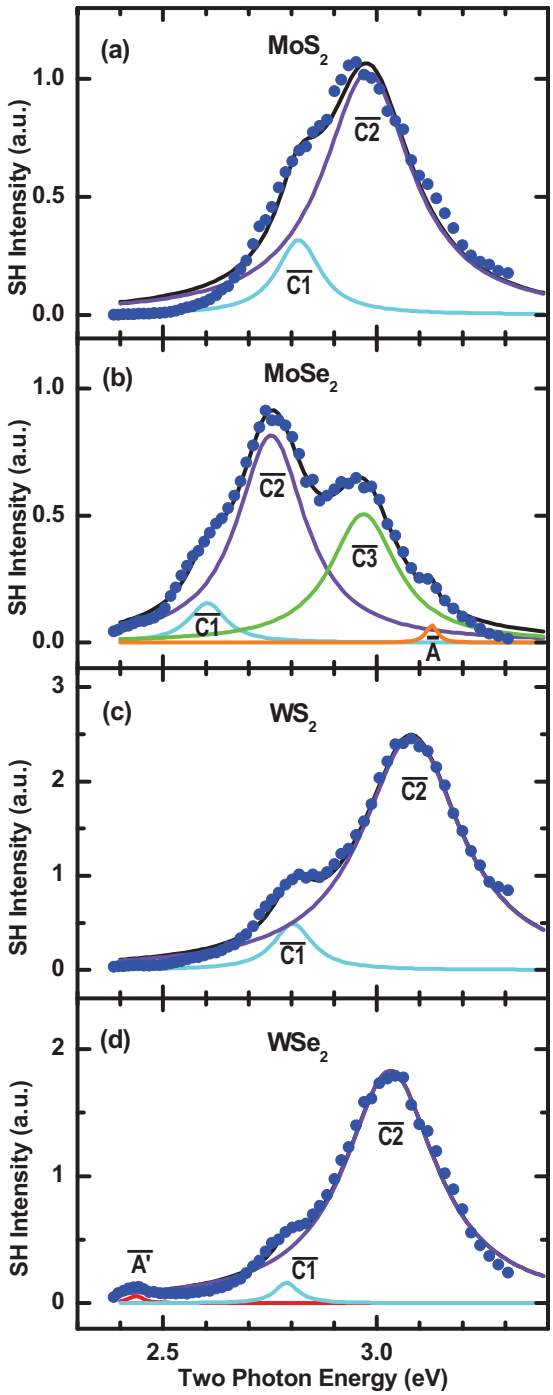


FIG. 1. SHG spectra of monolayer (a) $MoS_2$, (b) $MoSe_2$, (c) $WS_2$, and (d) $WSe_2$ on $SiO_2$ (90 nm)/Si(001) substrates. Blue dots: experimental spectra. Black lines: spectra fitted by the linear combination of Lorentz functions. Colored lines: spectra of the component Lorentzians.

where $\omega_i$, $\Gamma_i$, and $f_i$ are the resonance frequency, damping frequency, and amplitude of each component, respectively [49,50]. This formula does not include cross terms; i.e., the phase of each term is not considered. The reason for this is as follows. The resonance curves shown in Fig. 1 are associated with the C peak in the DR spectra, as described later. The C peak does not originate from a single optical transition but arises from a number of transitions at critical points in the Brillouin zone. Therefore, the components of the SHG spectra are also associated with a number of transitions; thus, the phase cannot be defined for each term in Eq. (1). The components thus obtained are indicated by colored lines in Fig. 1. The SHG spectra of $MoS_2$, $MoSe_2$, $WS_2$, and $WSe_2$ are decomposed into two, four, two, and three components, respectively. The dominant features common to the four $TX_2$ materials are the largest and broadest (full width at half

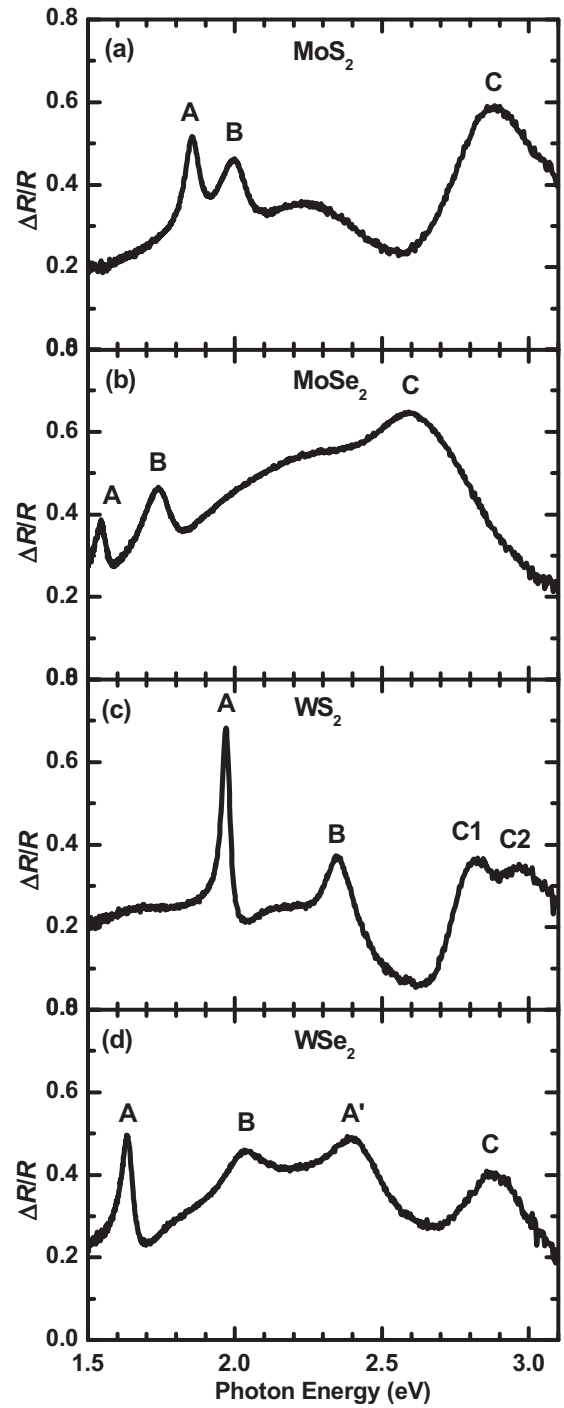


FIG. 2. DR spectra of monolayer (a) $MoS_2$, (b) $MoSe_2$, (c) $WS_2$, and (d) $WSe_2$ on $SiO_2$ (90 nm)/Si(001) substrates.

maximum ≈ 0.2–0.3 eV) component (violet line) and a small component on its low-energy side (sky-blue line), which are denoted as $\overline{C2}$ and $\overline{C1}$, respectively. For $MoSe_2$, there are two additional components on the high-energy side of $\overline{C2}$. They are denoted as $\overline{C3}$ (green line) and $\overline{A}$ (orange line), respectively. For $WSe_2$, there is a weak component denoted $\overline{A'}$ (red line) on the low-energy side of $\overline{C1}$. The origin of these components will be discussed after the description of the DR spectra.

The DR spectra of monolayer $TX_2$ are shown in Figs. 2(a)–2(d). For all the $TX_2$ materials, the A and B peaks at lower photon energies (below 2.5 eV) are generally ascribed to excitonic features associated with interband transitions from spin-orbit split valence bands at the $K$ and $K'$ points in the Brillouin zone [15,16,22]. Broad C peaks at higher energies (above 2.5 eV) were assigned to optical transitions at critical points according to theoretical calculations [21,51,52]. In the assignment, the critical points in a ring-shaped area around the Γ point, particularly along the $\Gamma-K/K'$ line, make a major contribution, while those in the vicinity of the $K$ and $K'$ points make a minor contribution. In any case, these critical points are formed as a result of band nesting, which means that there are energy regions where the conduction and valence bands are parallel to each other. Then, Van Hove singularities around the transition energies at the critical points, especially logarithmic divergence in the two-dimensional system, appear in the JDOS spectrum, giving rise to a strong optical response. The peak C splits into two peaks C1 and C2 in $WS_2$, as previously reported [53]. For $WSe_2$, an additional peak is observed between B and C. This peak is attributed to the low-energy peak A′ of the exciton pair (A′, B′) in the bulk [20] according to the thickness dependence of the peak energies [15,54]. This pair was initially interpreted to be split from the exciton pair (A, B) by an interlayer interaction arising from the overlap between the Se p orbitals of adjacent layers [55]. However, the peak A′ is observed even in the monolayer, which means that it does not originate only from the interlayer interaction. Thus, the origin of the peak A′ remains an open question.

The peak energies of the components of the SHG spectra and the peak energies of the DR spectra are summarized in Tables I(a) and I(b), respectively. The C peaks of the DR spectra for $MoS_2$, $MoSe_2$, and $WSe_2$ are located between the $\overline{C1}$ and $\overline{C2}$ components of the SHG spectra. For $WS_2$, the C1 and C2 peaks roughly coincide with the $\overline{C1}$ and $\overline{C2}$ components, respectively. Thus, the $\overline{C1}$ and $\overline{C2}$ components dominating the SHG spectra are naturally assigned to the two parts of the optical transitions responsible for the C peaks. The overall feature of the $\overline{C1}$ and $\overline{C2}$ components is common to the four $TX_2$ materials, which implies that the optical transitions responsible for these components and therefore the originating electronic structure are similar among the four $TX_2$ materials. Moreover, the C peaks are closer to the smaller component $\overline{C1}$ than to the larger component $\overline{C2}$, which means that the SH intensity at the $\overline{C2}$ component is considerably higher than that at the $\overline{C1}$ component. Now, we compare our SHG spectrum with the calculation results for $MoS_2$ in Ref. [41], because the calculation included both the spin-orbit interaction and the electron-hole interaction, and the presented optical conductivity and SHG spectra were well resolved in the interband transition region. The SHG spectrum exhibits an apparent peak at 3.0 eV and a weak shoulder at 2.8 eV, which correspond to the lower peak at 2.95 eV and the higher peak at 2.75 eV in the optical conductivity spectrum, respectively. Thus, the SH intensity at 3.0 eV is significantly higher than that at 2.8 eV. The calculation results therefore agree with our SHG spectra with regard to both the peak energies and the relative intensities.

Although the optical transitions responsible for these peaks were not assigned in Ref. [41], inferences about the transitions can be drawn from the present SHG spectra with the aid of the published results of calculations related to the linear optical spectra in the interband transition region [21,51,52]. There are two possibilities. One possibility is that the $\overline{C1}$ and $\overline{C2}$ components correspond to transitions from spin-orbit split valence bands around the same $k$ point, because the energy separations between the $\overline{C1}$ and $\overline{C2}$ peaks in $WX_2$ are approximately 1.7 times larger than those in $MoX_2$; similarly, the energy separations between the spin-orbit split A and B peaks in $WX_2$ are approximately 2.3 times larger than those in $MoX_2$. In this case, the $k$ point is considered to be located in the vicinity of the $K$ and $K'$ points because the spin-orbit splitting of the valence bands is the largest at these points. The interpretation is consistent with the fact that the overall feature of the $\overline{C1}$ and $\overline{C2}$ components is common to the

TABLE I. (a) Peak energies (eV) of the components of the SHG spectra of monolayer $TX_2$. (b) Peak energies (eV) of the DR spectra of monolayer $TX_2$.

(a)

| | $\overline{A}$ | $\overline{C1}$ | $\overline{C2}$ | $\overline{C3}$ | $\overline{A'}$ |
|---|---|---|---|---|---|
| $MoS_2$ | | $2.817 \pm 0.010$ | $2.978 \pm 0.007$ | | |
| $MoSe_2$ | | $2.603 \pm 0.007$ | $2.753 \pm 0.002$ | $2.969 \pm 0.003$ | $3.128 \pm 0.006$ |
| $WS_2$ | | $2.804 \pm 0.005$ | $3.081 \pm 0.002$ | | |
| $WSe_2$ | $2.436 \pm 0.001$ | $2.789 \pm 0.009$ | $3.031 \pm 0.002$ | | |

(b)

| | A | B | A′ | C or C1 | C2 |
|---|---|---|---|---|---|
| $MoS_2$ | 1.85 | 2.00 | | 2.87 | |
| $MoSe_2$ | 1.55 | 1.74 | | 2.60 | |
| $WS_2$ | 1.97 | 2.34 | | 2.81 | 2.98 |
| $WSe_2$ | 1.63 | 2.05 | 2.42 | 2.88 | |

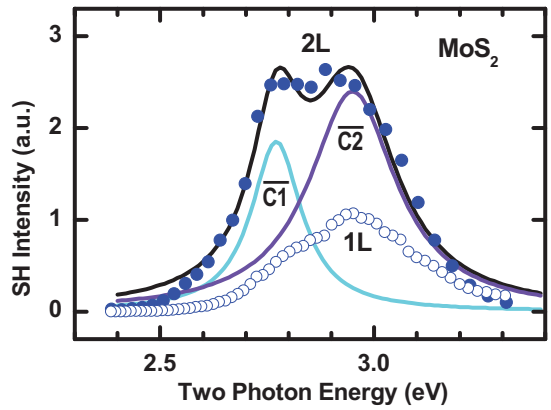


FIG. 3. SHG spectra of double layer (2L) $MoS_2$ on $SiO_2$ (90 nm)/Si(001) substrates. Blue dots: experimental spectrum. Black line: spectrum fitted by the linear combination of Lorentz function. Colored lines: spectra of the component Lorentzians. The experimental spectrum of monolayer (1L), which is the same as that in Fig. 1(a), is also plotted with blue circles for comparison.

four $TX_2$ materials. However, the considerably higher SH intensity for the $\overline{C2}$ component seems to conflict with this interpretation, because the transitions from spin-orbit split states are expected to induce a doublet with similar intensities in the SHG spectra, similar to the transitions responsible for the A and B excitons [33,34,38,41]. Another possibility is that the transitions contributing to the $\overline{C2}$ and $\overline{C1}$ components occur at different $k$ points where the spin-orbit splitting of the valence bands is small. These $k$ points are away from the $K$ and $K'$ points because the spin-orbit splitting deceases to zero as the $k$ point goes to the Γ or $M$ points. The $k$ points are thus considered to be located in a ring-shaped area around the Γ point. This interpretation is consistent with the calculation results for the linear optical spectra and with the considerably higher SH intensity at the $\overline{C2}$ component.

It is difficult to declare which possibility is plausible if we only consider the SHG spectra of monolayer. Accordingly, we measured SHG spectrum of bilayer $MoS_2$ to examine how the interlayer interaction affects the $\overline{C2}$ and $\overline{C1}$ components, because it is known that the valence-band maximum (VBM) at the Γ point is very sensitive to the interlayer interaction, but both the VBM and the conduction-band minimum (CBM) at the $K$ point is insensitive [56,57]. The sensitivity to the interlayer interaction was explained in terms of the constituent wave functions [56]: Wave functions of VBM at the Γ point shows lobes extend out from the sulfur atoms, while those of the VBM and CBM at the $K$ point are localized within the transition metal sublattice. The corrected SHG spectrum of bilayer $MoS_2$ on 90-nm-thick $SiO_2$ coated Si (001) substrates is indicated by blue dots in Fig. 3. SH intensity from most of bilayer area was nearly zero because SHG is symmetrically forbidden for 2H stacking. However, SH intensity from some bilayer area probably having 3R-type stacking was stronger than that from monolayer area [25,58]. The spectrum indicated by blue dots is the SHG spectrum of such bilayer area, and compared with the SHG spectrum of monolayer $MoS_2$ (blue circles). The SHG spectra of bilayer and monolayer $MoS_2$ have apparently different intensities and

TABLE II. (a) Peak energies (eV) of the components of the SHG spectra of bilayer (2L) and monolayer (1L) $MoS_2$. Fitted values for monolayer are the same as those in Table I(a). (b) Intensities of the components $f_i^2$ of the SHG spectra of of bilayer (2L) and monolayer (1L) $MoS_2$.

| | (a) | |
|---|---|---|
| | $\overline{C1}$ | $\overline{C2}$ |
| 2L | $2.771 \pm 0.007$ | $2.949 \pm 0.011$ |
| 1L | $2.817 \pm 0.010$ | $2.978 \pm 0.007$ |
| | (b) | |
| | $\overline{C1}$ | $\overline{C2}$ |
| 2L | $0.098 \pm 0.019$ | $0.192 \pm 0.022$ |
| 1L | $0.035 \pm 0.012$ | $0.129 \pm 0.009$ |

different spectrum shapes. In order to quantitatively analyze these features, the SHG spectrum of bilayer was fitted by a linear combination of Lorentz functions [Eq. (1)] in the same way as the SHG spectra of monolayers. The $\overline{C1}$ and $\overline{C2}$ components thus obtained are indicated by colored lines in Fig. 3. Resultant peak energies and intensities for these components of bilayer and monolayer spectra are summarized in Table II. As the layer changes from monolayer to bilayer, peak energies of these components shift to lower energies only slightly, but the intensity-ratio of $\overline{C1}$ to $\overline{C2}$ remarkably increases from 0.27 to 0.51. This result will explain the low energy shift of the peak of the SHG spectra [31] and probably that of the DR spectra [24]. It is noteworthy that the energy shift of the unresolved peak does not mainly arise from the energy shift of the components but from their intensity change. The interpretation of the bilayer spectrum is based on the hypothesis that the transitions contributing to the $\overline{C1}$ and $\overline{C2}$ components are the same in bilayer and monolayer. However, it is fair to mention that the hypothesis should be verified by the optical spectrum calculation of 3R-type stacked bilayer $MoS_2$ in future. In any case, electronic structures responsible for $\overline{C2}$ and $\overline{C1}$ components are found to be very sensitive to the interlayer interaction. Accordingly, we conclude that the optical transitions contributing to the $\overline{C2}$ and $\overline{C1}$ components occur at different $k$ points located in a ring-shaped area around the Γ point.

The $\overline{C3}$ component is observed on the high-energy side of the $\overline{C2}$ component in $MoSe_2$. The SH intensity for the $\overline{C3}$ component appears to be as high as that for the $\overline{C2}$ component. According to Ref. [52], there is a third peak—denoted as E—on the high-energy side of the two peaks Ca and Cb for $MoSe_2$. The E peak originates from the transitions around the middle of $K$-$M$ and Γ-$K$. Thus, the $\overline{C3}$ component may be assigned to these transitions. In this way, the $\overline{C1}$, $\overline{C2}$, and $\overline{C3}$ components are ascribed to the two-photon resonance with the transitions at various critical points in the Brillouin zone. The C peaks in the DR spectra were resolved in the SHG spectra. That is, the components of a multicomponent spectrum were better distinguished in the nonlinear optical spectra than in the linear optical spectra. The phenomenon resembles the case of the $SiO_2$/Si(001) interface, where $|\chi^{(2)}|$ resonances around $E_1$- and $E_2$-type critical points are sharper

than the $|\chi^{(1)}|$ spectrum [49]. The reason for this phenomenon is probably that the SHG spectra measured in this study are for a specific element ($\chi^{(2)}_{xyy}$) of the $\chi^{(2)}$ tensor, and the responsible transitions are more restricted by polarization-dependent selection rules than the transitions contributing to $\chi^{(1)}$, as in the case of the $SiO_2$/Si(111) interface [59]. In any case, the previously observed difference between the SHG spectra and the DR spectra for $MoS_2$ [31] is readily explained by the multicomponent nature of the C peak, that is, by the fact that the optical transitions contributing to the $\overline{C2}$ component induce a stronger nonlinear optical response than those contributing to the $\overline{C1}$ component.

The $\overline{A}$ component in $MoSe_2$ is ascribed to one-photon resonance at the A exciton, because half of the peak energy of $\overline{A}$ is 1.56 eV, which is almost the same as the energy of the A exciton. The $\overline{A'}$ component in $WSe_2$ is ascribed to two-photon resonance at the A′ exciton, because the peak energy of $\overline{A'}$, 2.44 eV, is the same as the energy of the A′ exciton. Notably, the intensities of the $\overline{A}$ and $\overline{A'}$ components are at least one order lower than those of the $\overline{C2}$ component. Thus, it is proven that the interband resonance is significantly stronger than the excitonic resonance, although the SHG spectra have been studied intensively in the exciton region rather than in the interband transition region.

## IV. CONCLUSION

The SHG spectra of four monolayer $TX_2$ materials were measured in the two-photon energy region of 2.4–3.3 eV. The spectrum of each $TX_2$ material exhibited noteworthy multiple peaks and was decomposed into a few components using a linear combination of Lorentz functions. The spectrum shape of the main $\overline{C1}$ and $\overline{C2}$ components was identical among the four $TX_2$ materials, which implies that the electronic structure responsible for these components was common among the four $TX_2$ materials. The SH intensity for the $\overline{C2}$ component was considerably higher than that for the $\overline{C1}$ component, which agrees with the published results of the SHG spectrum calculation for $MoS_2$. The optical transitions contributing to these components were concluded to occur at different $k$ points in a ring-shaped area around the Γ point with the aid of the SHG spectrum of bilayer $MoS_2$. Thus, the main components in the SHG spectra, that is, $\overline{C1}$ and $\overline{C2}$ (and $\overline{C3}$ for $MoSe_2$), are ascribed to two-photon resonance with the interband transitions at various critical points formed as a result of band nesting. Additional components, that is, $\overline{A}$ in $MoSe_2$ and $\overline{A'}$ in $WSe_2$, are ascribed to one-photon resonance at the A exciton and two-photon resonance at the A′ exciton, respectively. The intensities of the $\overline{A}$ and $\overline{A'}$ components were at least one order lower than those of the $\overline{C1}$ and $\overline{C2}$ (and $\overline{C3}$ for $MoSe_2$) components. Therefore, the interband resonance was directly proven to be significantly stronger than the excitonic resonance. The strong nonlinear optical response in the interband transition region and the detailed interpretation of its generation mechanism elucidated in this study could be important in the future application of monolayer $TX_2$ to nonlinear optical devices.

*Note added in proof.* Very recently Mokim *et al.* reported SHG spectra of monolayer $WS_2$ and $WSe_2$ measured by a new single-shot second harmonic (SH) method using broadband near-infrared femtosecond continuum pulses [60]. Their spectra are quite different from ours measured by the well established conventional point-by-point laser tuning SH spectroscopic method.


[1] K. S. Novoselov, A. K. Geim, S. V. Morozov, D. Jiang, Y. Zhang, S. V. Dubonos, I. V. Grigorieva, and A. A. Firsov, Science **306**, 666 (2004).

[2] K. Alam and R. K. Lake, IEEE Trans. Electron Devices **59**, 3250 (2012).

[3] M. Chhowalla, H. S. Shin, G. Eda, I. Li, K. P. Loh, and H. Zhang, Nat. Chem. **5**, 263 (2013).

[4] A. K. Geim and I. V. Grigorieva, Nature (London) **499**, 419 (2013).

[5] B. Radisavljevic, A. Radenovic, J. Brivio, V. Giacommetti, and A. Kis, Nat. Nanotechnol. **6**, 147 (2011).

[6] Q. H. Wang, K. Kalanter-Zadeh, A. Kis, J. N. Coleman, and M. S. Strano, Nat. Nanotechnol. **7**, 699 (2012).

[7] H. S. Lee, S. W. Min, Y. G. Chang, M. K. Park, T. Nam, H. Kim, J. H. Kim, S. Ryu, and S. Im, Nano Lett. **12**, 3695 (2012).

[8] R. S. Sundaram, M. Engel, A. Lombardo, R. Krupke, A. C. Ferrari, P. Avouris, and M. Steiner, Nano Lett. **13**, 1416 (2013).

[9] C. Lee, H. Yan, L. E. Brus, T. F. Heintz, J. Hone, and S. Ryu, ACS Nano **4**, 2695 (2010).

[10] A. Molina-Sanchez and L. Wirtz, Phys. Rev. B **84**, 155413 (2011).

[11] K. F. Mak, C. Lee, J. Hone, J. Shan, and T. F. Heintz, Phys. Rev. Lett. **105**, 136805 (2010).

[12] A. Splendiani, L. Sun, Y. Zhang, T. Li, J. Kim, C. Y. Chim, G. Galli, and F. Wang, Nano Lett. **10**, 1271 (2010).

[13] T. Cao, G. Wang, W. Han, H. Ye, C. Zhu, J. Shi, Q. Niu, P. Tan, E. Wang, B. Liu, and J. Feng, Nat. Commun. **3**, 887 (2012).

[14] K. F. Mak, K. He, J. Shan, and T. F. Heintz, Nat. Nanotechnol. **7**, 494 (2012).

[15] W. Zhao, Z. Ghorannevis, L. Chu, M. Toh, C. Kloc, P. H. Tan and G. Eda, ACS Nano **7**, 791 (2013).

[16] Y. Li, A. Chernikov, X. Zhang, A. Rigosi, H. M. Hill, A. M. van der Zande, D. A. Chenet, E.-M. Shih, J. Hone, and T. F. Heinz, Phys. Rev. B **90**, 205422 (2014).

[17] A. Ramasubramaniam, Phys. Rev. B **86**, 115409 (2012).

[18] H. Shi, H. Pan, Y.-W. Zhang, and B. I. Yakobson, Phys. Rev. B **87**, 155304 (2013).

[19] A. Molina-Sánchez, D. Sangalli, K. Hummer, A. Marini, and L. Wirtz, Phys. Rev. B **88**, 045412 (2013).

[20] J. A. Wilson and A. D. Yoffe, Adv. Phys. **18**, 193 (1969).

[21] A. Carvalho, R. M. Ribeiro, and A. H. Castro Neto, Phys. Rev. B **88**, 115205 (2013).

[22] D. Kozawa, R. Kumar, A. Carvalho, K. K. Amara, W. Zhao, S. Wang, M. Toh, R. M. Ribeiro, A.H. Castro Neto, K. Matsuda, and G. Eda, Nat. Commun. **5**, 4543 (2014).

[23] N. Kumar, S. Najmaei, Q. Cui, F. Ceballos, P. M. Ajayan, J. Lou, and H. Zhao, Phys. Rev. B **87**, 161403(R) (2013).

[24] Y. Li, Y. Rao, K. F. Mak, Y. You, S. Wang, C. R. Dean, and T. F. Heinz, Nano Lett. **13**, 3329 (2013).

[25] T. Jiang, H. Liu, D. Huang, S. Zhang, Y. Li, X. Gong, Y.-R. Shen, W.-T. Liu, and S. Wu, Nature Nanotech. **9**, 825 (2014).
[26] X. Zhang, C. Lin, Y. Tseng, K. Huang, and Y. Lee, Nano Lett. **15**, 410 (2015).
[27] M.-Y. Li, Y. Shi, C.-C. Cheng, L.-S. Lu, Y.-C. Lin, H.-L. Tang, M.-L. Tsai, C.-W. Chu, K.-H. Wei, Jr-H. He, W.-H. Chang, K. Suenaga, and L.-J. Li., Science **349**, 524 (2015).
[28] H. Zeng, G.-B. Liu, J. Dai, Y. Yan, B. Zhu, R. He, L. Xie, S. Xu, X. Chen, W. Yao, and X. Cui, Sci. Rep. **3**, 1608 (2013).
[29] C. Janisch, Y. Wang, D. Ma, N. Mehta, A. L. Elías, N. P. López, M. Terrones, V. Crespi, and Z. Liu, Sci. Rep. **4**, 5530 (2014).
[30] K. He, N. Kumar, L. Zhao, Z. Wang, K. F. Mak, H. Zhao, and J. Shan, Phys. Rev. Lett. **113**, 026803 (2014).
[31] L. M. Malard, T. V. Alencar, A. P. M. Barboza, K. F. Mak, and A. M. de Paula, Phys. Rev. B **87**, 201401(R) (2013).
[32] D. J. Clark, V. Senthilkumar, C. T. Le, D. L. Weerawarne, B. Shim, J. I. Jang, J. H. Shim, J. Cho, Y. Sim, M.-J. Seong, S. H. Rhim, A. J. Freeman, K.-H. Chung, and Y. S. Kim, Phys. Rev. B **90**, 121409(R) (2014).
[33] D. J. Clark, C. T. Le, V. Senthilkumar, F. Ullah, H.-Y. Cho, Y. Sim, M.-J. Seong, K.-H. Chung, Y. S. Kim, and J. I. Jang, Appl. Phys. Lett. **107**, 131113 (2015).
[34] G. Wang, I. C. Gerber, L. Bouet, D. Lagarde, A. Blocchi, M. Vidal, E. Palleau, T. Amand, X. Marie, and B. Urbaszek, 2D Mater. **2**, 045005 (2015).
[35] D. H. Kim and D. Lim, J. Korean Phys. Soc. **66**, 816 (2015).
[36] Z. Ye, T. Cao, K. O'Brien, H. Zhu, X. Yin, S. G. Louie, and X. Zhang, Nature (London) **513**, 214 (2014).
[37] J. Xiao, Z. Ye, Y. Wang, H. Zhu, Y. Wang, and X. Zhang, Light: Sci. Appl. **4**, e366 (2015).
[38] G. Wang, X. Marie, I. Gerber, T. Amand, D. Lagarde, L. Bouet, M. Vidal, A. Balocchi, and B. Urbaszek, Phys. Rev. Lett. **114**, 097403 (2015).
[39] K. L. Seyler, J. R. Schaibley, P. Gong, P. Rivera, A. M. Jones, S. Wu, J. Yan, D. G. Mandrus, W. Yao, and X. Xu, Nature Nanotech. **10**, 407 (2015).
[40] M. Grüning and C. Attaccalite, Phys. Rev. B **89**, 081102(R) (2014).
[41] M. L. Trolle, G. Seifert, and T. G. Pedersen, Phys. Rev. B **89**, 235410 (2014).
[42] S. H. Rhim, Y. S. Kim, and A. J. Freeman, Appl. Phys. Lett. **107**, 241908 (2015).
[43] C.-Y. Wang and G.-Y. Guo, J. Phys. Chem. C **119**, 13268 (2015).
[44] Y. Miyauchi, R. Morishita, M. Tanaka, S. Ohno, G. Mizutani, and T. Suzuki, J. Appl. Phys. **55**. 085801 (2016).
[45] M. Tanaka, H. Fukutani, and G. Kuwabara, J. Phys. Soc. Jpn. **45**, 1899 (1978).
[46] See Supplemental Material at http://link.aps.org/supplemental/10.1103/PhysRevB.100.075301 for transmission spectra of beam splitters.
[47] Y. Y. Wang, Z. H. Ni, Z. X. Shen, H. M. Wang, and Y. H. Wu, Appl. Phys. Lett. **92**, 043121 (2008).
[48] See Supplemental Material at http://link.aps.org/supplemental/10.1103/PhysRevB.100.075301 for enhancement factor spectrum of the $TX_2/SiO_2/Si$ system.
[49] G. Erley and W. Daum, Phys. Rev. B **58**, R1734 (1998).
[50] T. Suzuki, Phys. Rev. B **61**, R5117 (2000).
[51] D. Y. Qiu, F. H. da Jornada, and S. G. Louie, Phys. Rev. Lett. **111**, 216805 (2013).
[52] R. Gillen and J. Maultzsch, IEEE J. Sel. Top. Quantum Electron. **23**, 219 (2017).
[53] H. M. Hill, A. F. Rigosi, C. Roquelet, A. Chernikov, T. C. Berkelbach, D. R. Reichman, M. S. Hybertsen, L. E. Brus, and T. F. Heinz, Nano Lett. **15**, 2992 (2015).
[54] A. Arora, M. Koperski, K. Nogajewski, J. Marcus, C. Faugeras, and M. Potemski, NanoScale **7**, 10421 (2015).
[55] A. R. Beal, J. C. Knights, and W. Y. Liang, J. Phys. C **5**, 3540 (1972).
[56] H.-P. Komsa and A. V. Krasheninnikov, Phys. Rev. B **88**, 085318 (2013).
[57] J. Jeong, Y.-H. Choi, K. Jeong, H. Park, D. Kim, and M.-H. Cho, Phys. Rev. B **97**, 075433 (2018).
[58] W.-T. Hsu, Z.-A. Zhao, L.-J. Li, C.-H. Chen, M.-H. Chiu, P.-S. Chang, Y.-C. Chou, and W.-H. Chang, ACS Nano **8**, 2951 (2014).
[59] C. Meyer, G. Lüpke, U. Emmerichs, F. Wolter, H. Kurz, C. H. BJorkman, and G. Lucovsky, Phys. Rev. Lett. **74**, 3001 (1995).
[60] M. Mokim, A. Card, and F. Ganikhanov, MethodsX **6**, 910 (2019).

*Correction:* The *Note added in proof* requested at proof stage was not implemented properly and has now been set right.